

Blume-Emery-Griffiths model on Random Graphs

R. Erichsen Jr., Alexandre Silveira, S. G. Magalhães

Instituto de Física, Universidade Federal do Rio Grande do Sul, Cx. Postal 15051, 91501-970 Porto Alegre, RS, Brazil

Abstract

The Blume-Emery-Griffiths model with a random crystal field is studied in a random graph architecture, in which the average connectivity is a controllable parameter. The disordered average over the graph realizations is treated by replica symmetry formalism of order parameter functions. A self consistent equation for the distribution of local fields is derived, and numerically solved by a population dynamics algorithm. The results show that the average connectivity amounts to changes in the topology of the phase diagrams. Phase diagrams for representative values of the model parameters are compared with those obtained for fully connected mean field and renormalization group approaches.

Keywords: BEG model, Disordered systems, Finite connectivity

PACS: 64.60.De, 87.19.lj, 87.19.lg

1. Introduction

The three spin states ($\sigma = 0, \pm 1$) Blume-Emery-Griffiths (BEG) [1] was introduced with the aim to describe qualitatively superfluidity in ^3He - ^4He mixtures and phase separation. It is composed by three terms: the spin exchange interaction responsible by stabilizing a magnetic order, the local crystal field favoring non-active spin states $\sigma = 0$ and the non-local bi-quadratic interaction term favouring active spin state $\sigma = \pm 1$ in neighboring sites. The competition between these three mechanisms is responsible for giving rise to a complex phase diagram. For instance, it is expected as an outcome, a phase diagram with second and first-order phase transitions lines and multicritical points. This has motivated this model to be investigated using several methods, such as mean field theory [2], effective field theory [3], cluster variation method [4, 5], Monte Carlo simulations [6, 7, 8], Bethe lattice [9, 10, 11] and renormalization group with hierarchical lattices [12]. This interest in the BEG model raises the question of what might be the effects of disorder on it.

It is known that the presence of disorder might lead to changes in the boundary line order of the phase transitions and, consequently, affecting multicritical phase diagrams [13, 14]. In the case of the BEG model, disorder can be introduced in three ways: by choosing exchange interaction, crystal field or bi-quadratic exchange strengths as a random variable or even a combination of the previously mentioned possibilities. Each situation can describe different problems. For instance, the case of a random bi-quadratic exchange can be used in neural networks, where this term in the

Email addresses: rubem@if.ufrgs.br (R. Erichsen Jr.), huyarius@gmail.com (Alexandre Silveira), sgmagal@gmail.com (S. G. Magalhães)

BEG model becomes a learning rule [15, 16]. On the other hand, a random crystal field can be applied to the modeling mixtures ^3He - ^4He in porous medium such as aerogel [17, 18].

The three possibilities of disorder in the BEG model and its combinations have been treated also in several techniques, such as mean field, renormalization group, Bethe lattice, transfer matrix, cluster variation, effective field theory (see, for instance, Refs. [14, 19, 20, 21, 22, 23, 24, 25, 26, 27, 28, 29, 30, 31]). In the case of the random crystal field field displayed in Ref. [29], results coming from mean field approximation (i. e., with infinite dimension or coordination number) and real space renormalization group can be compared. This last technique is quite suitable to describe low dimensionality scenarios. The most important difference between the two techniques is the suppression of the first-order phase transition lines or their replacing by continuous ones obtained in the renormalization group. The random crystal field BEG model with anti-ferromagnetic (AF) bi-quadratic coupling constant in the Bethe lattice was investigated in ref. [23].

Our purpose with this work is to study the random crystal field BEG (RCBEG) model on the ensemble of poissonian random graphs. The random graph offers the average connectivity c as a continuous, controllable parameter, allowing to investigate the RCBEG model for different regimes, i.e., from large connectivity, close to the fully connected limit corresponding to the mean field approximation, till to the small connectivity situation. One can expect that might occur important changes as compared with the mean field results involving the replacement and/or disappearance of multicritical points in the phase diagrams as long as c decreases. Indeed, this kind of changes for small c has been confirmed in the Blume-Capel model [32, 33] with an added disorder given by a random field. In that model, it was found that variations in c produced drastic changes in the multicritical phase diagrams as compared with fully connected case [34]. Indeed, some multicritical points disappear when c decreases [35].

To sum over the realizations of the random graph, we use the replica symmetry theory of order parameter functions [36, 37, 38]. As frustration is absent in this model, we anticipate that the replica symmetry solution is exact for this purpose. The same equations for this problem can be derived by the cavity method [39] after taking the ensemble average [40]. We approach the problem considering that the lattice of spins is a random graph, where the connectivity is finite and the degree of a site is given by a Poisson distribution. Thus, we offer an alternative route to approach this problem. Also, we study simultaneously the presence of random crystal field disorder and the disorder of the lattice. As it has been shown, the connectivity has a crucial role in phase diagram topology [35, 41, 42], allowing to change the nature of transitions and critical points through a fine-tuning of the control parameter.

The paper is organized as follows. In Sec. 2 we describe our model and derive the fundamental equations using replica symmetry theory for finite connectivity systems. In Sec. 3 we explain the method to numerically calculate the distribution of fields, some examples of order parameters are shown and the behavior of the system is described by drawing phase diagrams for the thermodynamic phases. The conclusions can be found in Sec. 4.

2. Model and Replica Procedure

The model's Hamiltonian is

$$H(\boldsymbol{\sigma}) = -\frac{J}{c} \sum_{i < j} c_{ij} \sigma_i \sigma_j - \frac{K}{c} \sum_{i < j} c_{ij} \sigma_i^2 \sigma_j^2 + \sum_i \Delta_i \sigma_i^2, \quad (1)$$

where $\sigma \equiv \{\sigma_i\}, i = 1 \dots N$ denotes the state of the system, c_{ij} are independent, identically distributed random variables (i.i.d.r.v.) chosen from the distribution

$$p(c_{ij}) = \frac{c}{N} \delta(c_{ij} - 1) + \left(1 - \frac{c}{N}\right) \delta(c_{ij}), \quad (2)$$

indicating if the pair of spins i and j is connected ($c_{ij} = 1$) or not ($c_{ij} = 0$), with the constant c representing the mean connectivity. The local, random crystal fields Δ_i are i.i.d.r.v. chosen from the distribution

$$p(\Delta_i) = p \delta(\Delta_i - \Delta) + (1 - p) \delta(\Delta_i). \quad (3)$$

The constant K controls the strenght of the bi-quadratic couplings. Using the replica method we can write the disorder averaged free energy as

$$f(\beta) = - \lim_{N \rightarrow \infty} \frac{1}{\beta N} \lim_{n \rightarrow 0} \frac{1}{n} \log \langle Z^n \rangle_{\mathbf{c}, \Delta}, \quad (4)$$

where

$$Z^n = \sum_{\sigma_1 \dots \sigma_n} e^{-\beta \sum_{\alpha} H(\sigma_{\alpha})} \quad (5)$$

is the replicated partition function $\sigma_{\alpha}, \alpha = 1 \dots n$ denotes the state of replica α , $\langle \cdot \rangle_{\mathbf{c}, \Delta}$, with $\mathbf{c} \equiv \{c_{ij}\}$ and $\Delta \equiv \{\Delta_i\}$, denotes the disorder average. In the limit $c/N \rightarrow 0$, the average over c_{ij} gives

$$\langle Z^n \rangle = \sum_{\sigma_1 \dots \sigma_n} \langle e^{-\beta \sum_{\alpha, i} \Delta_i \sigma_{i\alpha}^2} \rangle_{\Delta} \exp \left[\frac{c}{2N} \sum_{i \neq j} \left(e^{\frac{\beta J}{c} \sum_{\alpha} \sigma_{i\alpha} \sigma_{j\alpha} + \frac{\beta K}{c} \sum_{\alpha} \sigma_{i\alpha}^2 \sigma_{j\alpha}^2} - 1 \right) \right]. \quad (6)$$

To transform into a single spin problem, order functions

$$P(\sigma) = \frac{1}{N} \sum_i \delta_{\sigma \sigma_i}, \quad (7)$$

which represent the probability of a replicated spin variable σ_i to assume the replica state σ , and their conjugated order functions $\hat{P}(\sigma)$, are introduced. The partition function can be rewritten as (see the appendix)

$$\begin{aligned} \langle Z^n \rangle = & \int \prod_{\sigma} d\hat{P}(\sigma) dP(\sigma) \exp N \left\{ \sum_{\sigma} \hat{P}(\sigma) P(\sigma) + \frac{c}{2} \sum_{\sigma \sigma'} P(\sigma) P(\sigma') \right. \\ & \times \left. \left(e^{\frac{\beta J}{c} \sum_{\alpha} \sigma_{\alpha} \sigma'_{\alpha} + \frac{\beta K}{c} \sum_{\alpha} \sigma_{\alpha}^2 \sigma'^2_{\alpha}} - 1 \right) + \log \sum_{\sigma} \langle e^{-\hat{P}(\sigma) - \beta \Delta \sum_{\alpha} \sigma_{\alpha}^2} \rangle_{\Delta} \right\}. \end{aligned} \quad (8)$$

In the thermodynamic limit the integral can be evaluated through the saddle-point method. We eliminate the $\hat{P}(\sigma)$'s through the saddle-point equations and rewrite the free-energy as

$$\begin{aligned} f(\beta) = & - \lim_{n \rightarrow 0} \frac{1}{\beta n} \text{Extr} \left\{ - \frac{c}{2} \sum_{\sigma \sigma'} P(\sigma) P(\sigma') \left(e^{\frac{\beta J}{c} \sum_{\alpha} \sigma_{\alpha} \sigma'_{\alpha} + \frac{\beta K}{c} \sum_{\alpha} \sigma_{\alpha}^2 \sigma'^2_{\alpha}} - 1 \right) \right. \\ & \left. + \ln \left\langle \sum_{\sigma} \exp \left[c \sum_{\sigma'} P(\sigma') \left(e^{\frac{\beta J}{c} \sum_{\alpha} \sigma_{\alpha} \sigma'_{\alpha} + \frac{\beta K}{c} \sum_{\alpha} \sigma_{\alpha}^2 \sigma'^2_{\alpha}} - 1 \right) - \beta \Delta \sum_{\alpha} \sigma_{\alpha}^2 \right] \right\rangle_{\Delta} \right\}, \end{aligned} \quad (9)$$

where Extr amounts to take the extreme of the expression between braces relatively to $P(\sigma)$, which gives the remaining saddle-point equations

$$P(\sigma) = \frac{1}{\mathcal{N}} \left\langle \exp \left[c \sum_{\sigma'} P(\sigma') \left(e^{\frac{\beta J}{c} \sum_{\alpha} \sigma_{\alpha} \sigma'_{\alpha} + \frac{K\beta}{c} \sum_{\alpha} \sigma_{\alpha}^2 \sigma'^2_{\alpha}} - 1 \right) - \beta \Delta \sum_{\alpha} \sigma_{\alpha}^2 \right] \right\rangle_{\Delta}, \quad (10)$$

where \mathcal{N} is a normalization factor.

We search solutions of Eq. (10) satisfying the RS Ansatz, where the order function is invariant under replica index permutations, which are written in the form

$$P(\sigma) = \int \mathcal{D}W(x, y) \frac{e^{\beta x \sum_{\alpha} \sigma_{\alpha} + \beta y \sum_{\alpha} \sigma_{\alpha}^2}}{\left(\sum_{\sigma} e^{\beta x \sigma + \beta y \sigma^2} \right)^n}, \quad (11)$$

where $\mathcal{D}W(x, y) \equiv dx dy W(x, y)$. Expanding the exponential of Eq. (10) and introducing Eq. (11) we obtain a self consistent equation for the distribution of local fields (details in the Appendix)

$$W(x, y) = \sum_{k=0}^{\infty} \frac{c^k e^{-c}}{k!} \left\langle \int \prod_{l=1}^k \mathcal{D}W(x_l, y_l) \delta \left[x - \frac{1}{\beta} \sum_l \phi(x_l, y_l) \right] \delta \left[y + \Delta - \frac{1}{\beta} \sum_l \psi(x_l, y_l) \right] \right\rangle_{\Delta}, \quad (12)$$

where

$$\phi(x, y) = \frac{1}{2} \ln \frac{\chi_{+1}(x, y)}{\chi_{-1}(x, y)}, \quad (13)$$

$$\psi(x, y) = \frac{1}{2} \ln \frac{\chi_{+1}(x, y) \chi_{-1}(x, y)}{\chi_0^2(x, y)}, \quad (14)$$

and

$$\chi_{\sigma}(x, y) = \sum_{\tau} e^{\beta x \tau + \frac{\beta}{c} J \sigma \tau + \beta y \tau^2 + \frac{\beta}{c} K \sigma^2 \tau^2}. \quad (15)$$

The relevant observables are the average magnetization

$$m = \sum_{\sigma} \sigma_{\alpha} P(\sigma) = \int \mathcal{D}W(x, y) \frac{2 \sinh(\beta x)}{e^{-\beta y} + 2 \cosh(\beta x)} \quad (16)$$

and the occupation number

$$Q = \sum_{\sigma} \sigma_{\alpha}^2 P(\sigma) = \int \mathcal{D}W(x, y) \frac{2 \cosh(\beta x)}{e^{-\beta y} + 2 \cosh(\beta x)}. \quad (17)$$

To determine the RS free-energy we insert the Ansatz (11) in Eq. (9) and take the limit $n \rightarrow 0$, which results

$$\begin{aligned} f(\beta) = & \frac{c}{2\beta} \int \mathcal{D}W(x, y) \mathcal{D}W(x', y') \frac{\sum_{\sigma \sigma'} e^{\beta x \sigma + \beta y \sigma^2 + \beta x' \sigma' + \beta y' \sigma'^2 + \frac{\beta}{c} J \sigma \sigma' + \frac{\beta}{c} K \sigma^2 \sigma'^2}}{\chi_0(x, y) \chi_0(x', y')} \\ & - \frac{1}{\beta} \sum_{k=0}^{\infty} P_k \int \prod_{l=1}^k \mathcal{D}W(x_l, y_l) \left\langle \ln \left(\sum_{\sigma} e^{-\beta \Delta \sigma^2} \prod_l \frac{\chi_{\sigma}(x_l, y_l)}{\chi_0(x_l, y_l)} \right) \right\rangle_{\Delta}, \end{aligned} \quad (18)$$

where $P_k = c^k e^{-c} / k!$ is a poissonian weight.

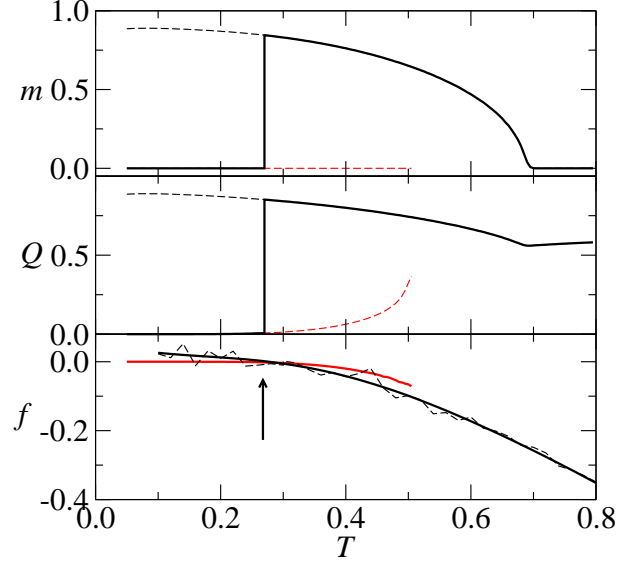


Figure 1: Magnetization m , occupation number Q and free-energy as functions of T for $p = 1$, $c = 8$, $K = 2$ and $D = 1.55$. Solid black lines on m and Q represent the stable order parameters values. Dashed black (dashed red) line represents metastable FM (PM) solution. Dashed black line on f is the metastable FM free-energy raw data. Solid black line is a polynomial adjust of the FM data. Solid red line is the PM free-energy data. The arrow signals the crossing of FM and PM free-energies.

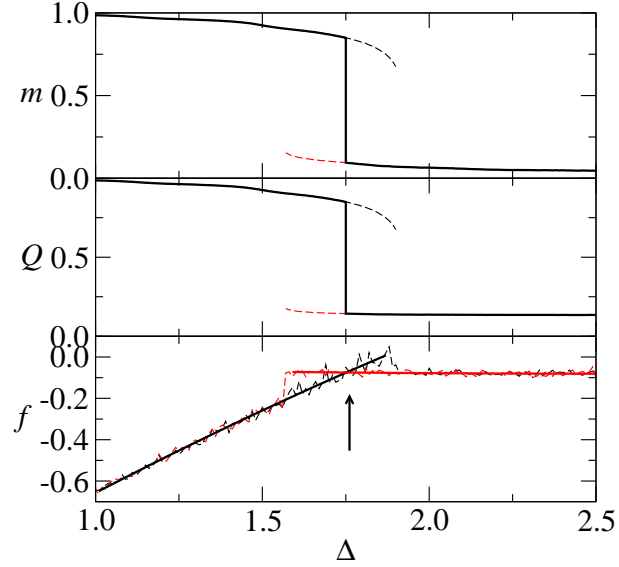


Figure 2: Magnetization m , occupation number Q and free-energy as functions of Δ for $p = 0.85$, $c = 8$, $K = 2$ and $T = 0.05$. Solid black lines on m and Q represent the stable order parameters values. Dashed black (dashed red) line represents metastable FM (PM) solution. Dashed black (red) line on f is the FM (PM) free-energy raw data. Solid black (red) line is a polynomial adjust of the FM (PM) data. The arrow signals the crossing of FM and PM free-energies.

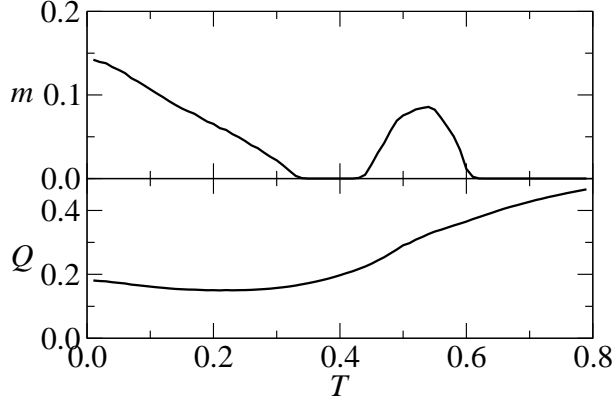


Figure 3: Magnetization m and occupation number Q as functions of T for $p = 0.85$, $c = 4$, $K = 2$ and $\Delta = 2.07$.

3. Results

According to Eqs. (16) – (18), the relevant order parameters are obtained through the calculation of the local field distribution, given by the self consistent equation (12). This is done numerically, via a population dynamics algorithm [39], as follows: (i) a population of \mathcal{N} two-component fields (x, y) is created; (ii) an integer k is randomly sorted from a Poisson distribution of mean c , and k fields are randomly chosen from the population; (iii) with the sorted fields, evaluate the two summations appearing in the delta functions of Eq. (12) and (iv) the results are assigned to the components of a further randomly chosen field (x^*, y^*) . The algorithm is repeated till the convergence to a stable population distribution $W(x, y)$. Throughout this work we used populations of $\mathcal{N} = 100,000$ fields and convergence time that amounts to 5,000,000 iterations. Still, each point is averaged over 20 runs. As shown in Eq. (18), the first free-energy term contains a double integral and the second term contains a k -fold integral over the local field distribution. To evaluate these terms, we follow a Montecarlo algorithm: a large number (1,000,000) of pairs and k -sets of local fields are randomly chosen and their contributions are summed. This results in a noisy curve, contrary to m and Q evaluations that contain a simple integral. To overcome the noise, the f curves are adjusted by a polynomial.

As example of the outcome, order parameters and free-energy curves are shown in Fig. 1, as functions of T , for $c = 8$, $K = 2$, $p = 1$ and $\Delta = 1.55$. Here and in the sequel the energy scale is fixed by assuming the bi-linear coupling constant $J = 1$. For $\Delta = 1.55$, PM and FM phases coexist from $T = 0$ till a continuous FM – PM transition at $T \approx 0.693$. To overcome the noisy free-energy and find the discontinuous transition locus we resort to a polynomial fit which indicates the crossing of the free-energy curves at $T \approx 0.266$. PM is stable in the $0 \leq T \lesssim 0.266$ and $0.693 \lesssim T$ interval. FM is stable in the $0.266 \lesssim T \lesssim 0.693$ interval. This characterizes a re-entrant behavior. The discontinuous transition at $T \approx 0.266$ appears as a dashed red line on Fig. 5a and continuous transition at $T \approx 0.693$ appears as a solid red line in the same figure.

Order parameters and free-energy curves as functions of the crystal field Δ , for $c = 8$, $K = 2$, $p = 0.85$ and $T = 0.05$ are shown in Fig. 2. The curves show a high m , high Q FM₁ phase at small Δ , a low m , low Q FM₂ at large Δ and a co-existence region between them. As mentioned above, we resort to a linear fit to find a crossing of the free-energy curves at $\Delta \approx 1.75$. This reveals a

discontinuous transition between the two ferromagnetic phases, represented by the dashed red line on Fig. 5b. The reason for the existence of two FM's phases will be discussed below.

The order parameters m and Q as functions of the temperature for $c = 4$, $p = 0.85$, $K = 2$ and $\Delta = 2.07$ are shown in Fig. 3. This figure shows, as the temperature increases, a FM₂ phase, then a re-entrant PM phase, a FM₂ phase and a PM phase at high T .

To give a complete overview of a model with so many parameters, keeping a reasonable amount of pictures, is a difficult task, and the zero-temperature K versus Δ phase diagram may guide us. This diagram is shown in Fig. 4 for the representative case $c = 4$ and $p = 0.85$, revealing a discontinuous FM₁ - FM₂ transition and a continuous FM₂ - PM transition. The two ferromagnetic phases are present, at low temperature, whenever $p < 1$, i.e., in the presence of disorder. This disorder acts turning off the crystal field Δ in a $1 - p$ fraction of sites, this way favouring the active states in these sites. The higher magnetization FM₁ is found at low Δ value, while the lower magnetization FM₂ and PM are found for higher Δ 's. Since the bi-quadratic coupling constant K favours the active states, higher magnetization phases are found as K increases. It is unnecessary to add further zero temperature diagrams, but it is worthy to mention that, as the connectivity c increases, or p decreases, FM₂ becomes stable at large Δ and there is no more a PM phase at $T = 0$.

To describe the finite temperature behavior, T versus Δ phase diagrams for $K = 2$ and $K = 5$ are presented in Figs. 5 and 6, respectively. For each K value results for representative disorder parameters $p = 1$, $p = 0.85$ and $p = 0.5$, as well as connectivity values $c = 4$ and $c = 8$, are shown. Results for $p = 0.5$ with $c = 25$ and $c = 100$ were also included, allowing for a better comprehension of the convergence to the mean field approach, which is expected for large c (see ref. [29]).

Smaller c values, like $0 < c < 1$ are below the percolation limit $c = 1$ preventing, thus, the appearing of ordered phases. This way, the solutions would be $m = 0$, $Q > 0$. The most interesting feature is the appearing of two paramagnetic phases, PM₁ and PM₂ (to be defined below), depending on parameters T and Δ .

The ordered case, $p = 1$ is shown in Figs. 5(a), for $K = 2$ and 6(a), for $K = 5$. If $K = 2$, there is a FM phase at low T , low Δ and a single PM phase elsewhere, with a continuous transition at high temperature, a re-entrant discontinuous transition at high Δ and a tricritical point (TCP) between them. TCPs, critical points (CPs) and critical end points (CEPs) are indicated as circles, squares and triangles in the figures. The re-entrant behavior is illustrated in Fig. 1, described above. If $K = 5$, in addition to the FM phase there are two paramagnetic phases, PM₁ and PM₂. The co-existence of PM₁ and PM₂ is typical of models with a non-magnetic state $\sigma = 0$, in which a sufficiently large crystal field suppresses the active $\sigma = \pm 1$ states. The high Q and low Q PM phases are named PM₁ and PM₂, respectively. The transition from FM to PM₁ is continuous, while the transition from PM₂ to FM and to PM₁ is discontinuous and re-entrant, with a CEP where the two lines meet. The PM₁ - PM₂ discontinuous transition ends at CP. The $p = 1$ diagrams are similar to those concerning the Bethe lattice approach reported in [9], although the re-entrant behavior in the discontinuous transition is more pronounced in the present paper. The re-entrant behavior in the ordered system with $K = 2$ was also reported in [29]. As a further remark, our results are qualitatively equivalent for both $c = 4$ and $c = 8$, although a lowering c appear to favour ordered phases.

Disorder, even for a moderate amount, i.e. $p = 0.85$, unfolds the ferromagnetic phase in two, namely FM₁ and FM₂. The first one is reminiscent of the ordered system's FM phase. The second one, located at low T and large Δ , arises consequently to disorder that turns off the crystal field in a fraction $1 - p$ of sites favouring the active states in these sites, as stated above. Connectivity effects become relevant. Figures 5(b) and 6(b) show that, for $c = 8$, FM₂ extends unbounded in Δ ,

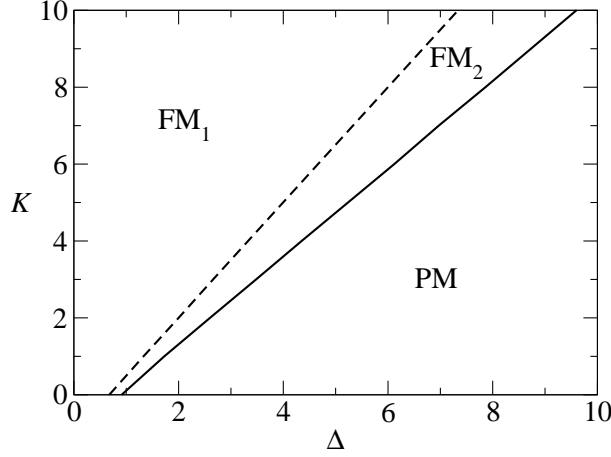


Figure 4: K versus Δ phase diagram for $T = 0$, $c = 4$ and $p = 0.85$. Solid (dashed) lines corresponds to continuous (discontinuous) transition.

in contrast to $c = 4$, where there appears a zero temperature PM phase. We argue that a moderate level of disorder is not a sufficient condition to stabilize a FM_2 phase at large Δ . Instead, it must be associated to a large cooperative FM neighborhood. This condition is found for $c = 8$, but it is not for $c = 4$. The random network with $c = 8$ and a moderate amount of disorder behaves similarly to a fully connected one, whose mean-field results are reported in [29]. In both models there is a part of the FM_1 - PM_2 that is discontinuous. In our case, although the finite connectivity, the random graph architecture still preserves a high dimensional nature. Conversely, renormalization group results for bi-dimensional systems, also reported in [29], show that this transition is entirely continuous. To end this part, additional qualitative differences between $K = 2$ and $K = 5$ for $p = 0.85$ should be reported. For $K = 2$, $c = 4$, there is a discontinuous FM_1 - FM_2 transition that ends in a CP, shown in the inset of Fig. 5(b). This way, the transition between the two FM phases and the PM is always continuous and re-entrant, as illustrated in Fig. 3. Conversely, for $K = 5$ and $c = 4$ there is a CEP and a TCP in the FM - PM transition, as shows Fig. 6(b). This figure also shows, detailed in the inset, for $c = 8$, a discontinuous PM_1 - PM_2 transition ending in a CP.

The scenario for a larger disorder, e.g. $p = 0.5$, is shown in Figs. 5(c) and 6(c) corresponding to $K = 2$ and $K = 5$, respectively. There is little to remark in these figures beyond the Δ -dependent continuous FM - PM transition. The expectation for lower p values is that the critical temperature approaches a constant $T \sim 1$ for all Δ . This behavior is significantly distinct from the mean-field description for high disorder [29]. To investigate the behavior of the highly disordered random network as c increases, the phase diagrams for $c = 25$ and $c = 100$, $K = 2$ and $K = 5$ were drawn, for $p = 0.85$. The results are shown in Figs. 5(d), for $K = 2$ and 6(d), for $K = 5$. The results show that the convergence to the fully connected scenario is faster for $K = 5$. For $c = 25$ the FM phase unfolds in FM_1 and FM_2 with a discontinuous transition between them ending in a CP. The fully connected scenario is observed for $c = 100$, with a CEP, a TCP and discontinuous FM_1 - PM transition between them.

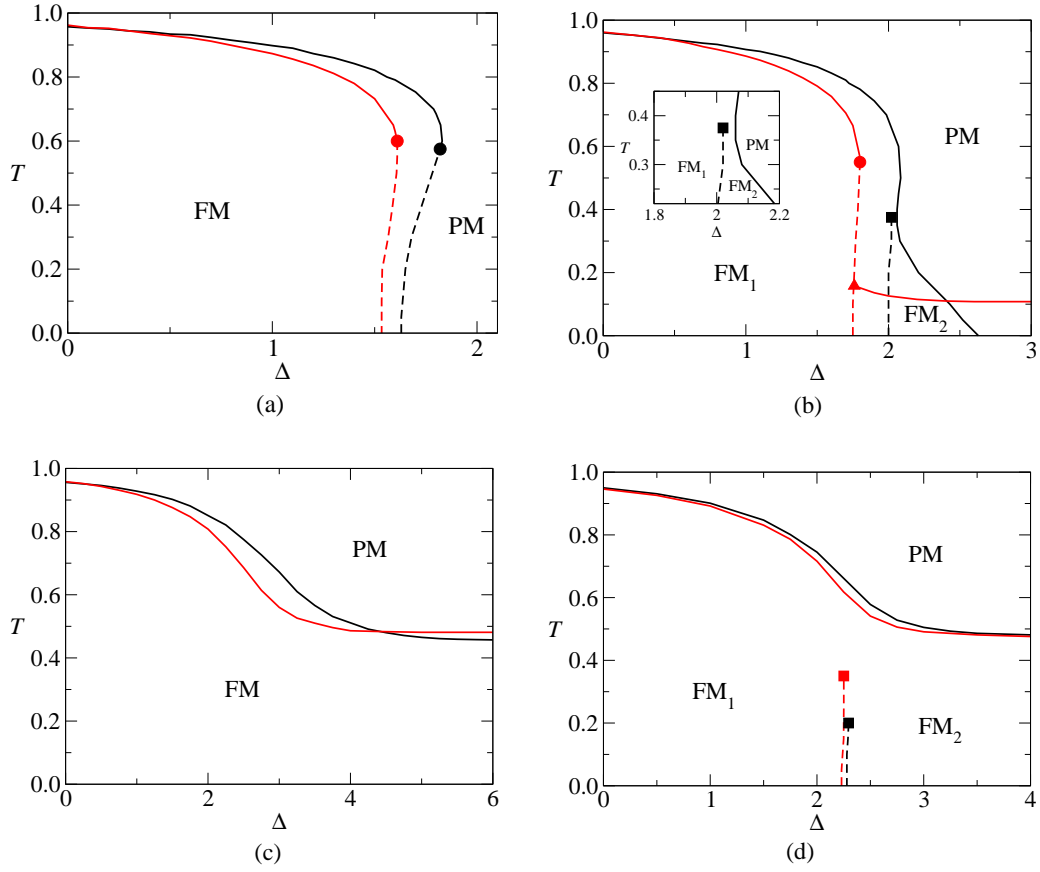


Figure 5: Thermodynamic phase diagrams T versus Δ for $K = 2$; (a) $p = 1$, (b) $p = 0.85$ and (c) $p = 0.5$. The inset in (b) shows in detail the vicinity of the critical point. The connectivity values are $c = 4$ (black) and $c = 8$ (red). (d) Thermodynamic phase diagrams for $p = 0.5$, $K = 2$, $c = 25$ (black), $c = 100$ (red). Solid (dashed) lines correspond to continuous (discontinuous) transitions. Circles, squares and triangles represent tri-critical points, critical points and critical end points, respectively

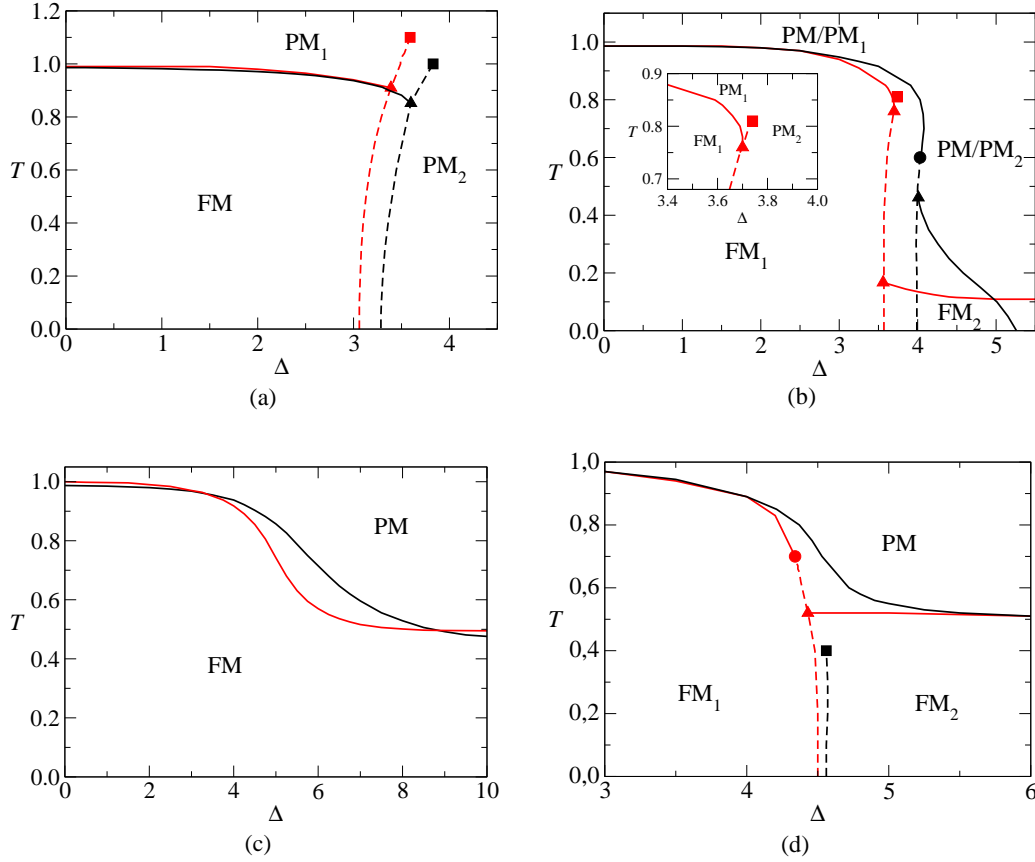


Figure 6: (a) Thermodynamic phase diagrams T versus Δ for $p = 1$, $K = 5$, $c = 4$ (black), $c = 8$ (red). (b) The same, but for $p = 0.85$; the inset shows in detail the vicinity of the critical points. (c) The same, but for $p = 0.5$. (d) Thermodynamic phase diagrams for $p = 0.5$, $K = 5$, $c = 25$ (black), $c = 100$ (red). Solid (dashed) lines correspond to continuous (discontinuous) transitions. Circles, squares and triangles represent tri-critical points, critical points and critical end points, respectively.

4. Conclusions

The BEG model with a disordered random crystal field was revisited, in a random graph topology, employing a finite connectivity technique. The disorder was introduced in the crystal field, as in [29] and through the random graph architecture. We argue that, instead the crystal field, disorder could be introduced in the bi-quadratic coupling constant and it would play a similar role. Our model for disorder ‘turns off’ the crystal field in a fraction of sites, allowing to this fraction to assume active states $\sigma = \pm 1$ without energetic penalty, even for large crystal field values.

Models with an inactive state $\sigma = 0$, like the ordered BEG model, unfolds the PM phase in a high temperature PM_1 and a low temperature PM_2 . The main role that the disorder plays is to unfold the FM phase in a high magnetization FM_1 and a low magnetization FM_2 . The last one survives at high crystal field values because the crystal field is ‘turned off’ in a finite fraction of sites. We fixed $K = 2$ and $K = 5$. Anti-ferromagnetic coupling constant $K < 0$, as reported in [23] for the Bethe lattice with fixed coordination number, allow for a richer thermodynamic scenario with the appearing of a quadrupolar staggered phase. To do the same in a random network architecture would require the introduction of a sub-network or a random network of clusters, and this remains in our scope for future works.

To end this work we resume the most relevant results. i) We found that the moderate disorder regime, e.g. $p = 0.85$, is the more sensitive to changes in the average connectivity, because the stabilization of FM_2 relies on the cooperative effect of a large neighborhood. Otherwise, for small c , a PM phase sets at low T and large Δ . This is the regime where the finite connectivity network becomes the more distinct from the fully connected one. ii) For a large disorder, like $p = 0.5$, the FM_1 - FM_2 discontinuous transition and the associated CP disappear at low c values, like $c = 4$ and $c = 8$, appearing for c as large as $c = 25$. iii) A phase diagram similar to the fully connected mean field description one only appears for $c = 100$ and $K = 5$, but not for $c = 100$ and $K = 2$. This suggests, in general lines, that some of the features observed in mean field phase diagrams are artifacts that does not exist in most of the real, finite connectivity physical systems.

Acknowledgements

The authors thanks to Dr. Nilton Branco for fruitful discussions and for carefully reading the manuscript. This work was supported, in part, by CNPq (Conselho Nacional de Desenvolvimento Científico e Tecnológico, Brazil).

Appendix: self consistent equation for the field distribution

The site spin variables appearing in the inner exponential of the replicated partition function, Eq. (6), are removed using the identity

$$1 = \prod_{\alpha=1}^n \sum_{\sigma_{\alpha}} \delta_{\sigma_{\alpha} \sigma_{\alpha i}} = \sum_{\sigma} \delta_{\sigma \sigma_i}, \quad (19)$$

where $\sigma = \{\sigma_1 \dots \sigma_n\}$ is a vector of replicated spin variables and σ_i is the replicated spin variable associated to spin i . Introducing the order functions $P(\sigma)$ through the identity

$$1 = \int \prod_{\sigma} dP(\sigma) \delta \left[P(\sigma) - \frac{1}{N} \sum_i \delta_{\sigma \sigma_i} \right], \quad (20)$$

Eq. (6) becomes

$$\begin{aligned} \langle Z^n \rangle = \sum_{\sigma_1 \dots \sigma_n} \int \prod_{\sigma} dP(\sigma) d\hat{P}(\sigma) \exp \left\{ \sum_{\sigma} \hat{P}(\sigma) P(\sigma) \right. \\ \left. + \frac{cN}{2} \sum_{\sigma \sigma'} P(\sigma) P(\sigma') \left(e^{\frac{\beta J}{c} \sum_{\alpha} \sigma_{\alpha} \sigma'_{\alpha} + \frac{\beta K}{c} \sum_{\alpha} \sigma_{\alpha}^2 \sigma'^2_{\alpha}} - 1 \right) \right. \\ \left. - \frac{1}{N} \sum_{\sigma} \hat{P}(\sigma) \sum_i \delta_{\sigma \sigma_i} \right\} \langle e^{-\beta \sum_{\alpha i} \Delta_i \sigma_{i\alpha}^2} \rangle_{\Delta}. \end{aligned} \quad (21)$$

Summing over the spin variables σ_i and changing variables $\hat{P}(\sigma) \rightarrow N\hat{P}(\sigma)$, Eq. (8) is obtained. Expanding the exponential in Eq. (10) and inserting the RS Ansatz, we obtain

$$P(\sigma) = \sum_{k=0}^{\infty} P_k \left\langle e^{-\beta \Delta \sum_{\alpha} \sigma_{\alpha}^2} \right\rangle_{\Delta} \int \prod_{l=1}^k \frac{\mathcal{D}W(x_l, y_l)}{\left(\sum_{\sigma} e^{\beta x_l \sigma_l + \beta y_l \sigma_l^2} \right)^n} \exp \sum_{\alpha=1}^n \ln \chi_{\sigma_{\alpha}}(x_l, y_l). \quad (22)$$

Now we withdraw the σ_{α} variables outside of the log using the identity $\sum_{\sigma} \delta_{\sigma \sigma_{\alpha}} = 1$,

$$\sum_{\alpha=1}^n \log \chi_{\sigma_{\alpha}}(x_l, y_l) = \sum_{\alpha=1}^n \sum_{\sigma} \delta_{\sigma \sigma_{\alpha}} \ln \chi_{\sigma}(x_l, y_l). \quad (23)$$

The Kronecker delta representation for the spin states $\sigma = \{-1, 0, 1\}$ is given by

$$\delta_{\sigma \sigma_{\alpha}} = 1 - \sigma^2 - \sigma_{\alpha}^2 + \frac{1}{2} \sigma \sigma_{\alpha} + \frac{3}{2} \sigma^2 \sigma_{\alpha}^2. \quad (24)$$

Summing over σ we get, after some algebra,

$$\begin{aligned} P(\sigma) = \sum_{k=0}^{\infty} P_k \left\langle \int \prod_{l=1}^k \frac{\mathcal{D}W(x_l, y_l)}{\left(\sum_{\sigma} e^{\beta x_l \sigma_l + \beta y_l \sigma_l^2} \right)^n} \exp \left\{ \left(\sum_{\alpha} \sigma_{\alpha} \right) \sum_{l=1}^k \phi(x_l, y_l) \right. \right. \\ \left. \left. + \left(\sum_{\alpha} \sigma_{\alpha}^2 \right) \sum_{l=1}^k \psi(x_l, y_l) - \left(\sum_{\alpha} \sigma_{\alpha}^2 \right) \beta \Delta \right\} \right\rangle_{\Delta}. \end{aligned} \quad (25)$$

Substitution of RS Ansatz in the LHS and taking the limit $n \rightarrow 0$

$$\begin{aligned} \int \mathcal{D}W(x, y) e^{\beta x \sum_{\alpha} \sigma_{\alpha} + \beta y \sum_{\alpha} \sigma_{\alpha}^2} = \int dx dy \left\{ \sum_{k=0}^{\infty} P_k \left\langle \int \prod_{l=1}^k \mathcal{D}W(x_l, y_l) \right. \right. \\ \left. \left. \times \delta \left[x - \beta^{-1} \sum_l \phi(x_l, y_l) \right] \delta \left[y + \Delta - \beta^{-1} \sum_l \psi(x_l, y_l) \right] \right\rangle_{\Delta} \right\} e^{\beta x \sum_{\alpha} \sigma_{\alpha} + \beta y \sum_{\alpha} \sigma_{\alpha}^2}. \end{aligned} \quad (26)$$

Comparing both sides of this equation we obtain Eq. (12).

References

- [1] M. Blume, V. J. Emery, and R. B. Griffiths, [Phys. Rev. A **4**, 1071 \(1971\)](#).

- [2] W. Hoston and A. N. Berker, [Phys. Rev. Lett. **67**, 1027 \(1991\)](#).
- [3] J. W. Tucker, [J. Phys.: Condens. Matter **1**, 485 \(1989\)](#).
- [4] G. Grigelionis and I. A. Rosengren, [Physica A **208**, 287 \(1994\)](#).
- [5] A. Rosengren and S. Lapinskas, [Phys. Rev. B **47**, 2643 \(1993\)](#).
- [6] Y.-L. Wang, F. Lee, and J. D. Kimel, [Phys. Rev. B **36**, 8945 \(1987\)](#).
- [7] Y. Wang and C. Wentworth, [J. Appl. Phys. **61**, 4411 \(1987\)](#).
- [8] K. Kasono and I. Ono, [Z. Phys. B Condens. Matter **88**, 213 \(1992\)](#).
- [9] A. Z. Akheyan and N. S. Ananikian, [J. Phys. A **29**, 721 \(1996\)](#).
- [10] K. Chakraborty and J. Tucker, [Physica A **137**, 122 \(1986\)](#).
- [11] R. Osorio, M. J. de Oliveira, and S. R. Salinas, [J. Phys.: Condens. Matter **1**, 6887 \(1989\)](#).
- [12] D. P. Snowman, [J. Magn. Magn. Mat. **321**, 3007 \(2009\)](#).
- [13] Y. Imry and S.-k. Ma, [Phys. Rev. Lett. **35**, 1399 \(1975\)](#).
- [14] K. Hui and A. N. Berker, [Phys. Rev. Lett. **62**, 2507 \(1989\)](#).
- [15] D. Bollé, D. R. C. Dominguez, R. Erichsen, E. Korutcheva, and W. K. Theumann, [Phys. Rev. E **68**, 062901 \(2003\)](#).
- [16] D. Bollé and J. Busquets Blanco, [Eur. Phys. J. B **47**, 281 \(2005\)](#).
- [17] A. Falicov and A. N. Berker, [Phys. Rev. Lett. **74**, 426 \(1995\)](#).
- [18] S. B. Kim, J. Ma, and M. H. W. Chan, [Phys. Rev. Lett. **71**, 2268 \(1993\)](#).
- [19] M. Sellito, M. Nocodemi, and J. Arenzon, [J. Phys. I France **7**, 945 \(1997\)](#).
- [20] E. Albayrak, [Physica B **479**, 107 \(2015\)](#).
- [21] E. Albayrak, [J. Magn. Magn. Mater. **386**, 20 \(2015\)](#).
- [22] H.-P. Dong and S.-L. Yan, [J. Magn. Magn. Mat. **308**, 90 \(2007\)](#).
- [23] J. Kple, F. Hontinfinde, and E. Albayrak, [J. Magn. Magn. Mat. **537**, 168217 \(2021\)](#).
- [24] J. Kple, F. Hontinfinde, and E. Albayrak, [Int. J. Theor. Phys. **59**, 3915 \(2020\)](#).
- [25] M. Karimou, E. Albayrak, A. Tessilimy, F. Hontinfinde, and R. Yessoufou, [Chin. J. Phys. **55**, 2371 \(2017\)](#).
- [26] H.-P. Dong and S.-L. Yan, [Commun. Theor. Phys. **49**, 511 \(2008\)](#).
- [27] H.-P. Dong and S.-L. Yan, [J. Magn. Magn. Mat. **308**, 90 \(2007\)](#).
- [28] H.-P. Dong and S.-L. Yan, [Solid State Commun. **139**, 406 \(2006\)](#).

- [29] N. S. Branco, [Phys. Rev. B **60**, 1033 \(1999\)](#).
- [30] C. Buzano, A. Maritan, and A. Pelizzola, [J. Phys.: Condens. Matter **6**, 327 \(1994\)](#).
- [31] A. Maritan, M. Cieplak, M. R. Swift, F. Toigo, and J. R. Banavar, [Phys. Rev. Lett. **69**, 221 \(1992\)](#).
- [32] M. Blume, [Phys. Rev. **141**, 517 \(1966\)](#).
- [33] H. Capel, [Physica **32**, 966 \(1966\)](#).
- [34] M. Kaufman and M. Kanner, [Phys. Rev. E **42**, 2378 \(1990\)](#).
- [35] R. Erichsen, A. A. Lopes, and S. G. Magalhaes, [Phys. Rev. E **95**, 062113 \(2017\)](#).
- [36] R. Monasson and R. Zecchina, [Phys. Rev. E **56**, 1357 \(1997\)](#).
- [37] R. Monasson and R. Zecchina, [J. Phys. A **31**, 9209 \(1998\)](#).
- [38] B. Wemmenhove and A. C. C. Coolen, [J. Phys. A **36**, 9617 \(2003\)](#).
- [39] M. Mézard and G. Parisi, [Eur. Phys. J. B **20**, 217 \(2001\)](#).
- [40] C. Lupo and F. Ricci-Tersenghi, [Phys. Rev. B **95**, 054433 \(2017\)](#).
- [41] R. Erichsen and W. K. Theumann, [Phys. Rev. E **83**, 061126 \(2011\)](#).
- [42] R. Erichsen, A. Silveira, and S. G. Magalhaes, [Phys. Rev. E **103**, 022133 \(2021\)](#).